

Article

# Efficient Removal of Pb(II) by Highly Porous Polymeric Sponges Self-Assembled from a Poly(Amic Acid)

Ying Leng <sup>1</sup>, Kai Jin <sup>1</sup>, Tian Wang <sup>2</sup> , Xiaoyong Lai <sup>1</sup> and Hui Sun <sup>1,\*</sup> 

<sup>1</sup> State Key Laboratory of High-Efficiency Coal Utilization and Green Chemical Engineering, School of Chemistry and Chemical Engineering, Ningxia University, Yinchuan 750021, China

<sup>2</sup> Department of Chemistry, University of Washington, Seattle, WA 98195, USA

\* Correspondence: sunhui@nxu.edu.cn

**Abstract:** Lead (II) (Pb(II)) is widespread in water and very harmful to creatures, and the efficient removal of it is still challenging. Therefore, we prepared a novel sponge-like polymer-based absorbent (poly(amic acid), PAA sponge) with a highly porous structure using a straightforward polymer self-assembly strategy for the efficient removal of Pb(II). In this study, the effects of the pH, dosage, adsorption time and concentration of Pb(II) on the adsorption behavior of the PAA sponge are investigated, revealing a rapid adsorption process with a removal efficiency up to 89.0% in 2 min. Based on the adsorption thermodynamics, the adsorption capacity increases with the concentration of Pb(II), reaching a maximum adsorption capacity of 609.7 mg g<sup>-1</sup> according to the Langmuir simulation fitting. Furthermore, the PAA sponge can be efficiently recycled and the removal efficiency of Pb(II) is still as high as 93% after five adsorption–desorption cycles. Fourier transform infrared spectroscopy and X-ray photoelectron spectroscopy analyses reveal that the efficient adsorption of Pb(II) by the PAA sponge is mainly due to the strong interaction between nitrogen-containing functional groups and Pb(II), and the coordination of oxygen atoms is also involved. Overall, we propose a polymer self-assembly strategy to easily prepare a PAA sponge for the efficient removal of Pb(II) from water.

**Keywords:** water remediation; Pb(II) adsorption; polymeric sponge; self-assembly; poly(amic acid)



**Citation:** Leng, Y.; Jin, K.; Wang, T.; Lai, X.; Sun, H. Efficient Removal of Pb(II) by Highly Porous Polymeric Sponges Self-Assembled from a Poly(Amic Acid). *Molecules* **2023**, *28*, 2897. <https://doi.org/10.3390/molecules28072897>

Academic Editor: Jianxun Ding

Received: 20 February 2023

Revised: 17 March 2023

Accepted: 22 March 2023

Published: 23 March 2023



**Copyright:** © 2023 by the authors. Licensee MDPI, Basel, Switzerland. This article is an open access article distributed under the terms and conditions of the Creative Commons Attribution (CC BY) license (<https://creativecommons.org/licenses/by/4.0/>).

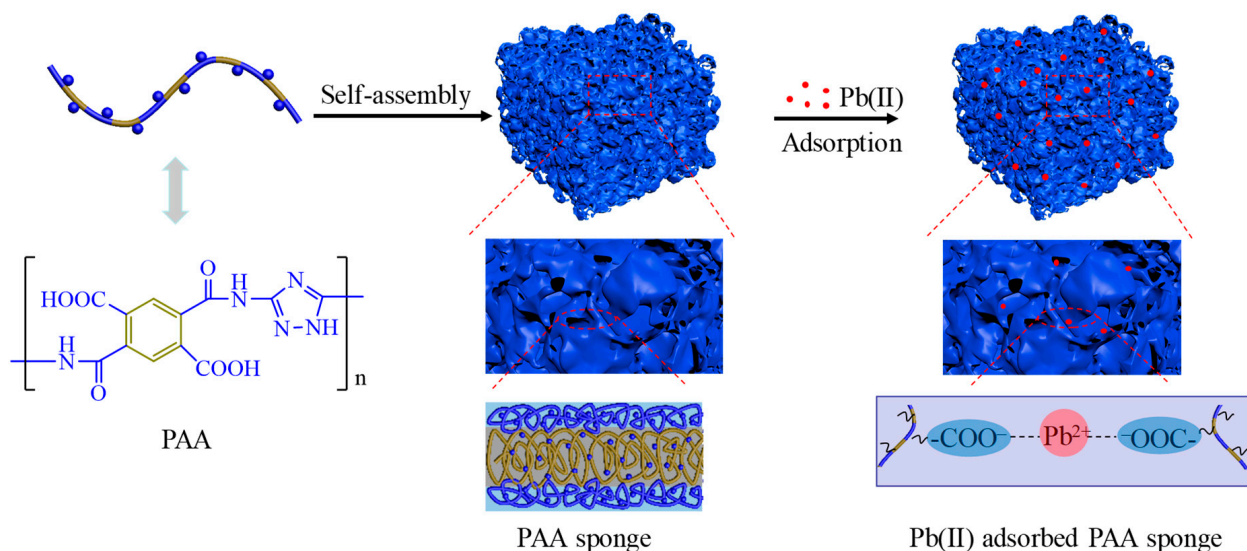
## 1. Introduction

Clean water is very important for the survival of plants and animals. However, with the rapid development of industrial and social modernization, the shortage of clean water and water pollution caused by various contaminants including dyes [1], polycyclic aromatic hydrocarbons (PAHs) [2] and heavy metal ions [3], etc., have brought severe global crises [4]. Among the many pollutants, heavy metal ions have drawn particular interest to scientific fields such as chemistry, nanotechnology and materials due to their features of widespread, persistent and high toxicity [5]. Lead (II) ion (Pb(II)) is considered one of the most harmful pollutants even at trace level concentration because of its widespread presence in the environment, accumulation and high toxicity to children [6]. If ingested in excess, lead can cause damage to the central nervous system, kidney, gastrointestinal, hematopoietic, cardiovascular and reproductive systems, and to brain function [7]. Therefore, the efficient removal of Pb(II) from water is of high urgency and great significance.

Various methods, including chemical precipitation, physical adsorption, ion exchange, membrane filtration, and so forth, are widely used to treat Pb(II) contaminated water [5,8–13], among which physical adsorption is one of the most efficient methods [14]. In comparison with the above-mentioned methods, physical adsorption is usually easy to carry out, cheap, recyclable and effective [5]. In particular, the rapid development of nanotechnology brings the opportunity for the booming of nano-adsorbents, which have emerged as one of the most promising candidates to remove Pb(II) from water [15]. A large amount of functional nanomaterials, including carbon-based nanomaterials, chitosan [16], metal–organic

frameworks (MOFs) [17–20], micelles [21,22], vesicles [23], magnetic nanoparticles [24–27], silica nanoparticles [28,29] and so forth, have been well developed to capture Pb(II) and other heavy metal ions from water. Recently, polymer self-assembly has been rapidly developed as a powerful tool to prepare functional nanomaterials [4,30–32]. For instance, our group presented a multifunctional homopolymer vesicle self-assembled from a scalable homopolymer, poly(amic acid) (PAA), to effectively remove four kinds of heavy metal ion ( $\text{Ni}^{2+}$ ,  $\text{Cu}^{2+}$ ,  $\text{Zn}^{2+}$ ,  $\text{Pb}^{2+}$ ) from wastewater [33]. However, it has always been hard to remove the nano-adsorbents from water after adsorption, which hinders the wider application of these functional nano-adsorbents.

Herein, we prepare a novel highly porous sponge-like nanostructure (PAA sponge) derived from the self-assembly of a poly(amic acid) (PAA) for the efficient removal of Pb(II) from water. As shown in Scheme 1, the amphiphilic alternating copolymer PAA was prepared by the condensation polymerization of two commercially available monomers, pyromellitic dianhydride (PMDA) and 3,5-diamino-1,2,4-triazole, under mild condition, which could self-assemble into nano-sponges with hydrophobic aromatic groups (yellow color) forming the framework and the hydrophilic moieties (blue color) covering the surface. Taking advantage of the high porosity and ultrathin frameworks of PAA sponge and functional groups that have high affinity with Pb(II), such as carboxylic and triazole groups, the PAA sponge shows excellent performance when removing Pb(II) from water via electrostatic interaction, coordination and chelation. Notably, more than 89.0% of Pb(II) can be removed from water within 2 min with a maximum adsorption capacity of  $609.7 \text{ mg g}^{-1}$ . In addition, FTIR and XPS were also used to confirm the strong interaction between Pb(II) and the functional groups.



**Scheme 1.** Schematic illustration of the preparation of the PAA sponge for the efficient adsorption of Pb(II). The blue dots represent the charged carboxylic group. The blue line represents the hydrophilic parts of PAA, while the yellow line represents the hydrophobic parts of PAA.

## 2. Results and Discussion

### 2.1. Synthesis and Self-Assembly of PAA

The synthesis of PAA was carried out according to our previous publication, as shown in Scheme S1 [34,35]. Fourier transform infrared spectroscopy (FTIR) and proton nuclear magnetic resonance ( $^1\text{H NMR}$ ) were conducted to confirm the structure of PAA (Figures S1 and S2) [34,35]. The PAA sponge was prepared by directly adding deionized water to the PAA solution ( $30 \text{ mg mL}^{-1}$ ), diluted by the stock solution with *N,N*-dimethylformamide (DMF). The organic solvent was removed by dialysis against deionized water, and the morphology of the PAA sponge was observed using a scanning electron microscope (SEM)

and a transmission electron microscope (TEM), demonstrating a sponge-like structure with high porosity and an ultrathin skeleton, as illustrated in Figure 1A–D. The formation process and the structure of the PAA sponge was proposed as follows: with the addition of deionized water to the DMF solution of PAA, the phase separation between the hydrophilic and hydrophobic parts of PAA drove the formation of very thin polymer membranes, as presented in Figure S3. Then, the thin membrane self-assembled into the PAA sponge with hydrophobic segments formed the skeleton and hydrophilic components covering the surface of the skeleton to maintain the colloidal stability by electrostatic repulsion (Scheme 1). The zeta potential of the PAA sponge was measured to be  $-28.2$  mV, demonstrating the strong negatively charged surface (Figure S4). The specific surface area of the PAA sponge was calculated to be  $23$  m<sup>2</sup> g<sup>-1</sup> (Figure S5A), and the existence of micro- and mesopores was also confirmed by TEM images (Figure 1C,D) and pore distributions in Figure S5B. The formation of the PAA sponge by the self-assembly of PAA with a highly porous structure and charged hydrophilic surface would be beneficial for the diffusion, sufficient contact and adsorption of Pb(II).

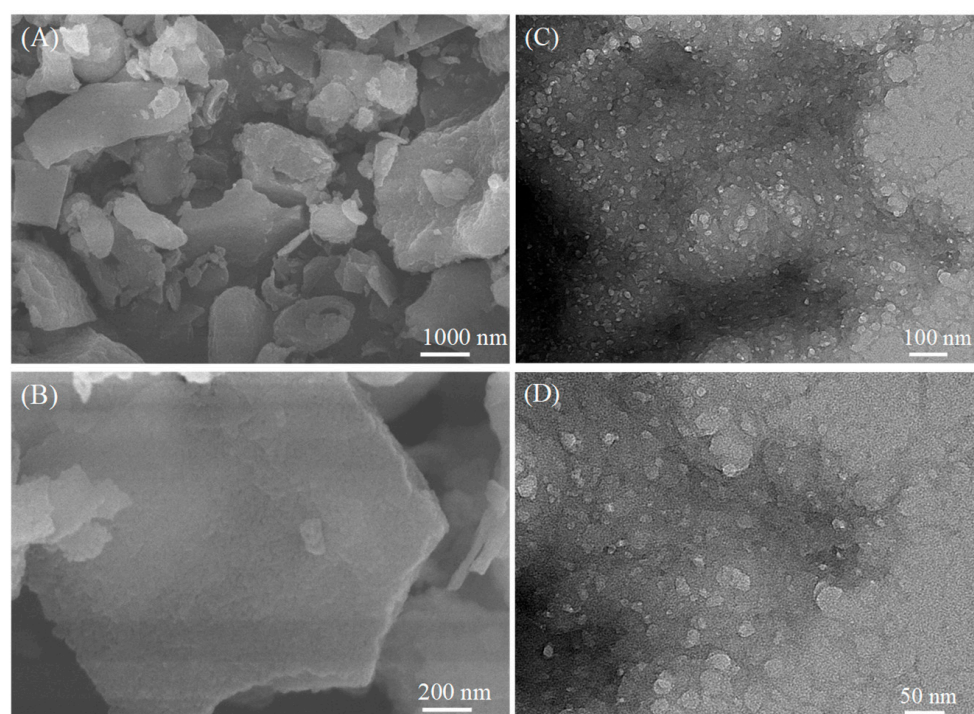


**Figure 1.** Morphology characterizations of PAA sponge: (A,B) SEM and (C,D) TEM images.

## 2.2. Effect of pH and PAA Sponge Dosage on Adsorption Performance

The pH of the solution is a key parameter that determines the adsorption performance toward heavy metal ions because of the surface charges and functional group chemistry of the adsorbent, which also has critical influence on the zeta potential and colloidal stability of the nanomaterials. As illustrated in Figure S6, when the solution is strongly acidic (pH 2), the zeta potential increased from  $-28.2$  to  $-17.8$  mV, implying the reduction of negative charges on the surface due to the protonation of carboxylic groups. With the increase of pH, part of carboxylic groups deprotonated, leading to the enhancement of negative charges on the surface of the PAA sponge, showing the decrease in zeta potentials (Figure S6). When the pH was 5, the zeta potential reached the minimum of  $-33.6$  mV, which would be beneficial for the adsorption of Pb(II) due to strong electrostatic interaction. Indeed, the adsorption capacity and removal efficiency also exhibited a similar trend, as shown in Figure 2A. When the pH of the solution was 2, the adsorption capacity and removal efficiency were only  $194.2$  mg g<sup>-1</sup> and 38.8%, respectively. With the increase of pH, the adsorption capacity and removal efficiency continuously increased to  $450.3$  mg g<sup>-1</sup> and

90.0% at pH 5, respectively. As the pH further increased to 6, the adsorption capacity and removal efficiency barely changed, demonstrating the saturation of adsorption due to the sufficient deprotonation of carboxylic groups. In addition, we also confirmed that the adjustment of the pH would not lead to the precipitation of Pb(II). The concentrations of lead(II) were 99.6 ppm and 100.3 ppm at pH 2 and 5, respectively, as measured by ICP-OES. Therefore, we conducted the following adsorption experiments at pH 5.

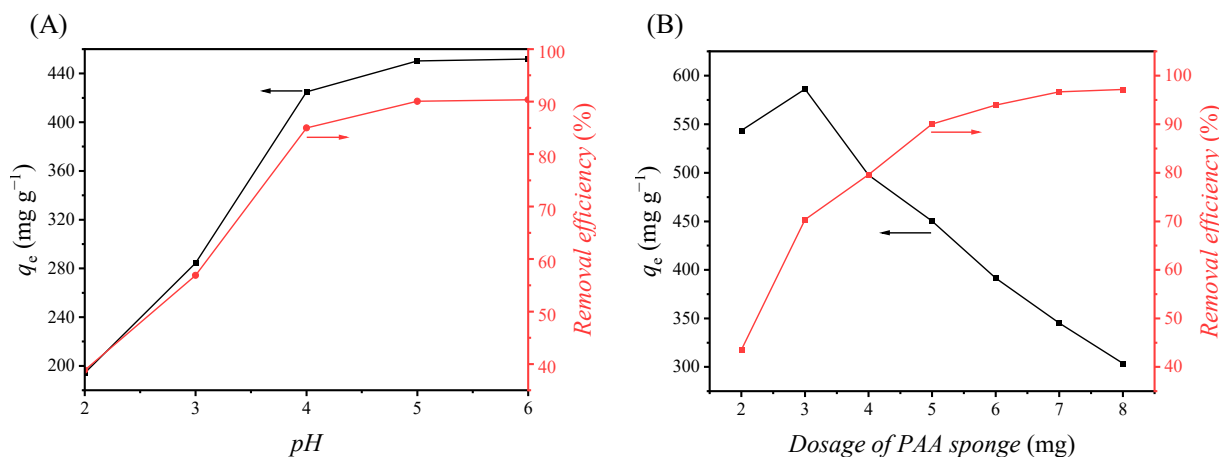


**Figure 2.** Effect of (A) pH and (B) dosage on the adsorption capacity at equilibrium ( $q_e$ ) and removal efficiency of the PAA sponge toward Pb(II).

The dosage of the PAA sponge also has an important impact on the adsorption behavior of Pb(II). As shown in Figure 2B, the adsorption capacity decreased with the dosage of the PAA sponge, while the removal efficiency showed the opposite trend. When the dosage of the PAA sponge was low ( $\leq 4.0$  mg), even if the adsorption capacity was pretty high (above  $500 \text{ mg g}^{-1}$ ) the removal efficiency was lower than 80%, demonstrating a residual concentration of Pb(II) still as high as 20.4 ppm. As the dosage of the PAA sponge increased to 6 mg, the removal capacity decreased to  $391.5 \text{ mg g}^{-1}$ , while the removal efficiency increased to 94.0%. With the further increase of the dosage to 8 mg, the removal efficiency reached 97.2% with an adsorption capacity of  $303.6 \text{ mg g}^{-1}$ , which is much better than previous studies [36–39], demonstrating the excellent adsorption performance of the PAA sponge towards Pb(II). It was noteworthy that the PAA sponge could be precipitated from the solution after adsorption due to the neutralization of the surface negative charges, as shown in Figure S7, which avoided the tedious removal procedures of nano-adsorbents.

### 2.3. Adsorption Kinetics

To further investigate the adsorption kinetics of Pb(II) ions by PAA sponge, the adsorption kinetics of Pb(II) were fitted by pseudo-first-order and pseudo-second-order kinetic models, respectively. The pseudo-first-order model described the initial stage of the adsorption process when the initial concentration was high, and the adsorbents had a few active sites. In that case, the external diffusion or the internal diffusion are the rate controlling step. The pseudo-second-order model reflects the final stage of the adsorption when the initial concentration is low. There are abundant active sites on the adsorbents, in which the adsorption kinetics are dominated by the adsorption onto the active site [40].

The pseudo-first-order kinetic model:

$$\ln(q_e - q_t) = \ln q_e - k_1 t \quad (1)$$

The pseudo-second-order kinetic model:

$$\frac{t}{q_t} = \frac{1}{q_e^2 k_2} + \frac{t}{q_e} \quad (2)$$

where  $q_t$  ( $\text{mg g}^{-1}$ ) and  $q_e$  ( $\text{mg g}^{-1}$ ) are the adsorption capacity of Pb(II) at time  $t$  (min) and equilibrium, respectively;  $k_1$  ( $\text{min}^{-1}$ ) and  $k_2$  ( $\text{g mg}^{-1} \text{min}^{-1}$ ) show the reaction rate constant of the pseudo-first-order and the pseudo-second-order kinetic models, respectively.

At the initial concentration of Pb(II) of 100 ppm and pH 5, the adsorption kinetics of Pb(II) by PAA sponge at different adsorption times were investigated. As shown in Figure S8, the adsorption process of Pb(II) was very fast. Additionally, the removal efficiency reached 89.0% with an adsorption capacity of  $370.7 \text{ mg g}^{-1}$  within 2 min, which we believe could be ascribed to the excellent water dispersability, highly porous structure and abundant functional groups on the surface of the PAA sponge, facilitating the fast adsorption of Pb(II). The adsorption reached equilibrium after 20 min with a removal efficiency of 91.7%. In order to investigate the adsorption kinetics quantitatively, we fitted the adsorption curve with pseudo-first-order and pseudo-second-order kinetic models, as illustrated in Figure 3A,B. Both the pseudo-first-order and pseudo-second-order kinetic models could be fitted well with the adsorption curve, showing excellent correlation. The fitting parameters are summarized in Table 1, and the correlation coefficient ( $R^2$ ) reached 0.9995 and 0.9998 for pseudo-first-order and pseudo-second-order kinetic models, respectively. In addition, the calculated  $q_e$  ( $378.3$  and  $381.4 \text{ mg g}^{-1}$ ) was also well fitted with the experimental result ( $378.4$ – $382.4 \text{ mg g}^{-1}$ ). Therefore, we can conclude that the adsorption of Pb(II) is dominated by both of physisorption and chemisorption [41].

**Table 1.** Adsorption kinetics parameters of the fitted pseudo-first-order and pseudo-second-order models.

Heavy Metal Ion	Pseudo-First-Order			Pseudo-Second-Order		
	$q_{e1}$ ( $\text{mg g}^{-1}$ )	$k_1$ ( $\text{min}^{-1}$ )	$R^2$	$q_{e2}$ ( $\text{mg g}^{-1}$ )	$k_2$ ( $\text{g (mg min)}^{-1}$ )	$R^2$
Pb(II)	379.3	1.892	0.9995	381.4	0.0413	0.9998

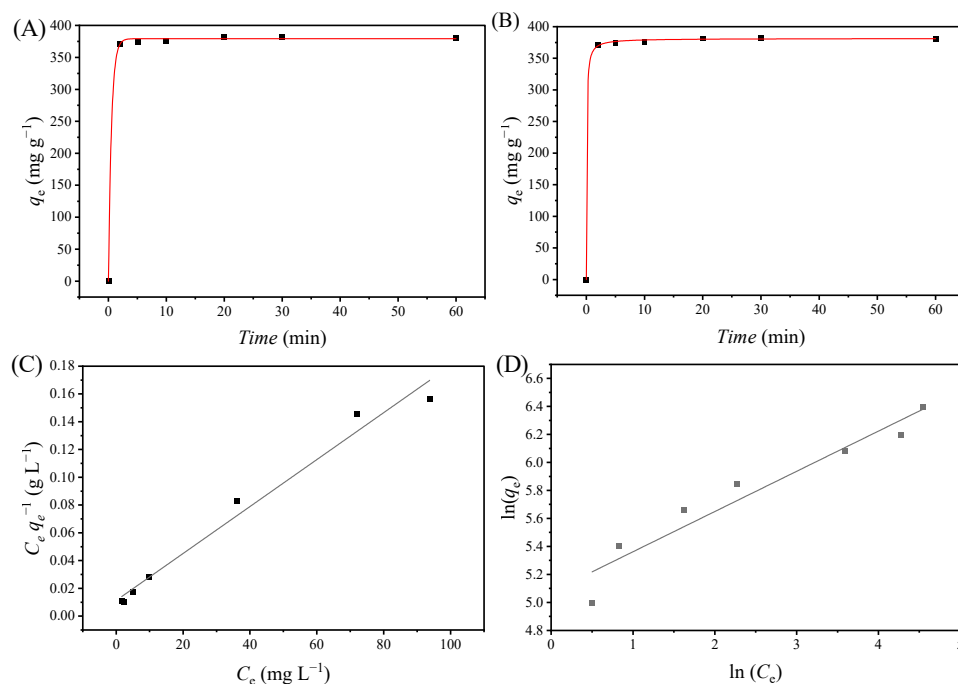


**Figure 3.** The adsorption kinetics of Pb(II) by PAA sponge fitted by (A) pseudo-first-order and (B) pseudo-second-order models, and the linear regression of the adsorption isotherm by fitting the equilibrium data with (C) the Langmuir and (D) the Freundlich adsorption models. The kinetic parameters and the thermodynamic parameters are presented in Tables 1 and 2.

**Table 2.** Isothermal parameters and correlation coefficient fitted by Langmuir and Freundlich models.

Heavy Metal Ion	Langmuir Isotherm			Freundlich Isotherm		
	$K_L$ (L mg <sup>-1</sup> )	$q_m$ (mg g <sup>-1</sup> )	$R^2$	$K_F$ (mg g <sup>-1</sup> (L mg <sup>-1</sup> ) <sup>1/n</sup> )	1/n	$R^2$
Pb(II)	0.1784	609.7	0.9972	118,700	0.2872	0.9304

#### 2.4. Adsorption Isotherms

The isothermal adsorption experiments were carried out at different concentrations of Pb(II) in order to depict the interaction pathway between the PAA sponge and Pb(II). The removal efficiency of the PAA sponge varied with the initial concentration of Pb(II), as shown in Figure S9. With the increase in the concentration of Pb(II), the adsorption capacity of the PAA sponge increased gradually, while the removal efficiency decreased obviously. The decrease in the removal efficiency of Pb(II) was due to the limited adsorption sites as the number of Pb(II) increased.

Furthermore, the Langmuir and Freundlich models were used to describe the adsorption and desorption isotherms of Pb(II). The Langmuir isotherm model assumes that the adsorption is monolayer and uniform, and also that there is no interaction between adsorbed molecules and the adsorption is dynamically at equilibrium [42]. The Freundlich model describes the adsorption equilibrium of a heterogeneous adsorbed surface [43].

$$\frac{C_e}{q_e} = \frac{1}{K_L q_m} + \frac{C_e}{q_m} \quad (3)$$

$$\log q_e = \log K_F C_e^{\frac{1}{n}} \quad (4)$$

where  $q_m$  (mg g<sup>-1</sup>) and  $q_e$  (mg g<sup>-1</sup>) represent the maximum removal capacity and the removal capacity at equilibrium, respectively;  $C_e$  is the Pb(II) concentration at equilibrium;  $K_L$  (L mg<sup>-1</sup>) is a Langmuir constant concerning adsorption energy; and  $n$  and  $K_F$  (mg g<sup>-1</sup> (L mg<sup>-1</sup>)<sup>1/n</sup>) represent the Freundlich constant associated with adsorption intensity and adsorption capacity, respectively.

Figure 3C,D and Table 2 show the fitted curves and isothermal parameters fitted by Langmuir and Freundlich models. The correlation coefficients of the Langmuir isotherm adsorption model ( $R^2 = 0.9972$ ) are higher than those of the Freundlich model ( $R^2 = 0.9304$ ), implying that the adsorption process could be well described by the Langmuir model [44]. Though the equilibrium adsorption data of Pb(II) by PAA sponge at 25 °C can be fitted well with the Langmuir model, it is still hard to describe the adsorption process with a single adsorption model considering the structural features and the abundant functional groups of the PAA sponge [45,46]. The adsorption process might happen in a mixed manner, and we confirmed the conclusion in the following text.

#### 2.5. Recyclability of the PAA Sponge

Efficient desorption is very important for the recyclability of adsorbents. Therefore, we evaluated the recyclability of the PAA sponge under acidic conditions to release the adsorbed Pb(II). As illustrated in Figure 4, the adsorbed Pb(II) could be effectively released from the PAA sponge as treated by 0.1 M HCl aqueous solution. The PAA sponge showed excellent recyclability for multiple adsorption–desorption cycles, and the removal efficiency was still as high as 93% after five cycles.

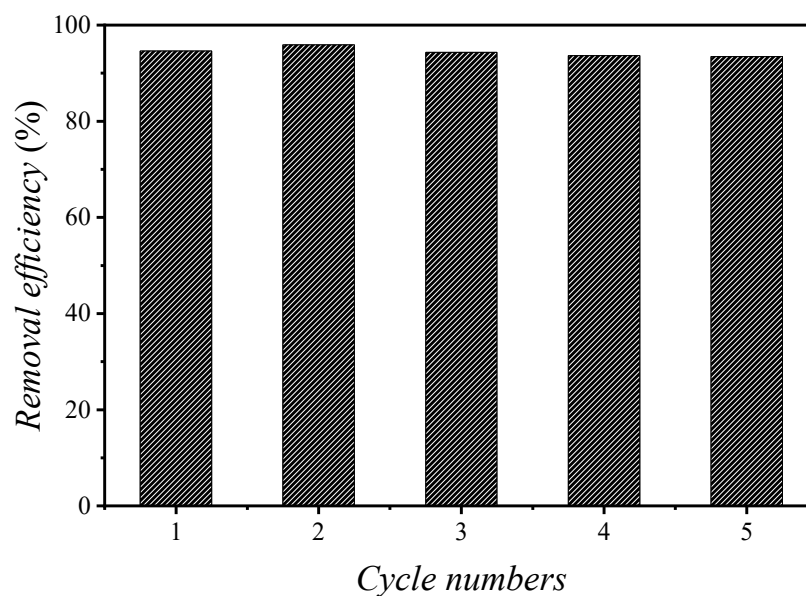


**Figure 4.** The recyclability of the PAA sponge after the adsorption of Pb(II).

#### 2.6. Mechanism for the Adsorption of Pb(II) by PAA Sponge

In order to understand the adsorption mechanism, FTIR spectra were obtained to analyze the changes in the characteristic absorption peaks of the functional groups before and after adsorption. As presented in Figure 5A, before the adsorption of Pb(II), the FTIR spectrum of the PAA sponge demonstrated that the adsorption peaks located at 1137, 1403, 1696, 3133 and 3417  $\text{cm}^{-1}$  represented the bond stretching of  $\text{CN}_{\text{ring}}$ , with stretching vibrations of C–N, C=O and C=N, O–H and N–H, respectively [47,48]. After the adsorption of Pb(II), the adsorption peak of C=N significantly weakened and shifted to 1118  $\text{cm}^{-1}$ , manifesting a strong interaction between the nitrogen species in the triazole ring and Pb(II), which could be further confirmed by the attenuation of the adsorption peak of N–H at 3417  $\text{cm}^{-1}$  [49]. In addition, the disappearance of the adsorption peak of O–H demonstrated the electrostatic interaction between Pb(II) and carboxylic groups [50]. Overall, we can conclude that Pb(II) is adsorbed into the PAA sponge due to the strong interaction between the nitrogen species in the triazole ring and Pb(II), and electrostatic interaction between the carboxylic group and Pb(II).

To further confirm the adsorption mechanism, XPS analysis was conducted to investigate the interaction between Pb(II) and nitrogen and oxygen species in the PAA sponge. Figure 5B shows the XPS survey spectrum of Pb(II) adsorbed by the PAA sponge. Comparing with the XPS survey spectrum in Figure S10, the appearance of the adsorption peak of Pb4f located at 138.4 eV demonstrated that Pb(II) was effectively adsorbed by the PAA sponge. Subsequently, the high resolution spectra of N1s and O1s before and after the adsorption of Pb(II) were also analyzed, as illustrated in Figure 5C,D. The adsorption peak of N1s of the PAA sponge before the adsorption of Pb(II) could be divided into two peaks, indicating the existence of two chemical states of nitrogen (Figure 5C). Additionally, the peaks which appeared at 399.52 and 400.74 eV were attributed to the tertiary amine and secondary amine, respectively [51]. After adsorption, a new peak was observed at a binding energy of 401.36 eV, suggesting that the adsorption mechanism relied on the complexation between the nitrogen atom and Pb(II), where a pair of electrons in the nitrogen atom was supplied to the shared bond between nitrogen and Pb(II) [52]. In addition, the shift in the binding energy of nitrogen species further explained the change in the chemical environment caused by the sharing of electrons between the nitrogen atom and Pb(II) [53]. In addition, the high-resolution spectra of Pb4f and C1s were also presented in Figures S11 and S12. The O1s spectra of the PAA sponge before and after the adsorption of Pb(II) are shown in Figure 5D. The adsorption peak could be divided into three peaks,

located at 531.39/531.25, 531.94/532.23 and 533.31/534.16 eV, which could be assigned to C=O, C–O and O–H bonds, respectively [54]. The shift and change in the intensity of the binding energy of the subdivided peaks proved that the coordination of Pb(II) with oxygen atoms occurred during adsorption [55]. Figure 6 vividly illustrates a possible adsorption mechanism between nitrogen atoms and the oxygen atoms of the PAA sponge forming strong coordination complexes with Pb(II). In summary, the efficient adsorption of Pb(II) by the PAA sponge was due to the synergy of physical adsorption and chemical adsorption.

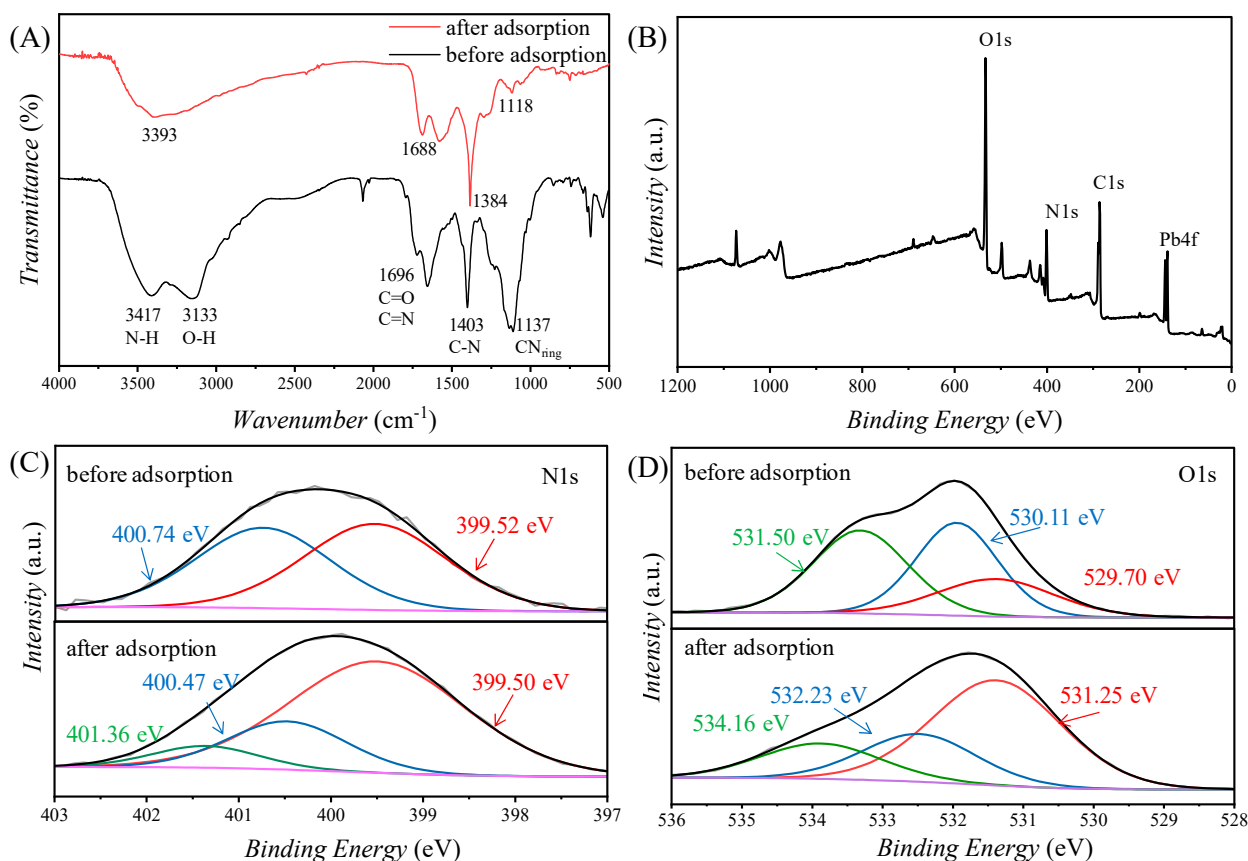


**Figure 5.** (A) FTIR spectra, (B) XPS survey and high resolution XPS spectra of (C) N1s and (D) O1s of PAA sponge after adsorption of Pb(II).

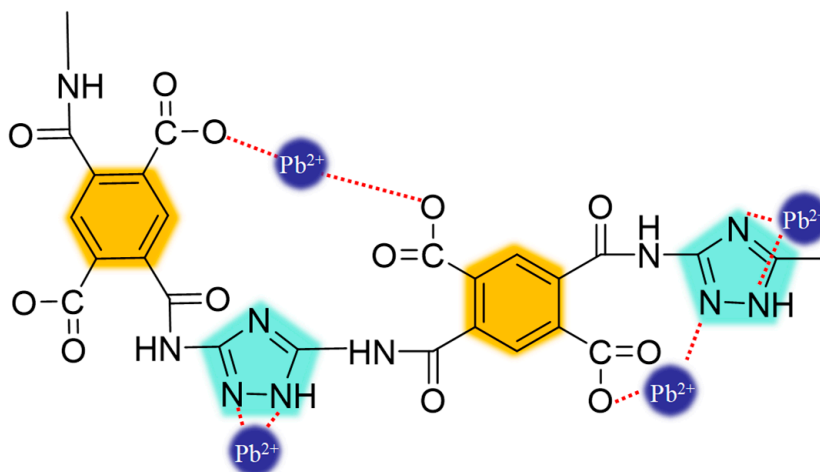


**Figure 6.** Schematic illustration of the adsorption mechanism of Pb(II) by PAA sponge.

### 3. Materials and Methods

#### 3.1. Materials

Pyromellitic dianhydride (PMDA, 99%) and 3,5-diamino-1,2,4-triazole (98%) were purchased from Aladdin Chemistry, Co., Ltd., Shanghai, China. DMSO- $d_6$  was purchased from J&K Scientific Ltd., Shanghai, China. *N,N*-Dimethylformamide (DMF, AR), acetone (AR), Sodium hydroxide (NaOH, 99.99%), hydrochloric acid (HCl, 35%) and lead nitrate ( $\text{Pb}(\text{NO}_3)_2$ , 99%) were purchased from Sinopharm Chemical Reagent Co., Ltd., Shanghai, China. and used as received.

#### 3.2. Experimental Section

##### 3.2.1. Synthesis of Poly(amic acid) (PAA)

To synthesize PAA, the 3,5-diamino-1,2,4-triazole (1.011 g, 10.00 mmol) dissolved in 20 mL of DMF was placed in an ice bath and the PMDA (2.204 g, 10.00 mmol) dispersion in 10 mL of DMF was added into the solution batch-by-batch in an hour. After stirring for another 2 h at ambient temperature, the polymerization was completed and the stock solution was obtained and stored at  $-20^\circ\text{C}$ . Subsequently, the stock solution was precipitated in acetone three times to afford PAA powder for further characterizations.

##### 3.2.2. Self-Assembly of the PAA into a Sponge

The PAA stock solution was diluted to  $30\text{ mg mL}^{-1}$  by DMF. Deionized water ( $v_{\text{water}}:v_{\text{DMF}} = 2:1$ ) was added dropwise to the PAA solution at a speed of  $5\text{ mL h}^{-1}$  by a peristaltic pump under stirring (250 rpm). DMF was removed by dialysis in deionized water. Then, the PAA sponge was obtained by freeze-drying under vacuum.

##### 3.2.3. Adsorption Experiments

Effect of pH values on the adsorption of Pb(II). In order to explore the influence of pH values on the adsorption of Pb(II), the pH values of Pb(II) aqueous solution (100 ppm, 25 mL) were adjusted with 0.1 M sodium hydroxide and hydrochloric acid. Subsequently, 5 mg of PAA sponge was added into the solution and stirred at 250 rpm for 24 h. All experiments were carried out at  $25^\circ\text{C}$ , and 2 mL of the mixture was taken out via syringe and filtered with a  $0.45\ \mu\text{m}$  filter. After that, the filtrate was collected for inductively coupled plasma optical emission spectrometer (ICP-OES) analysis. The adsorption capacity of the PAA sponge for Pb(II) ions can be evaluated according to the following equations:

$$q_e = \frac{(C_0 - C_t)V}{m} \quad (5)$$

$$\text{Removal efficiency} = \frac{C_0 - C_t}{C_0} \times 100\% \quad (6)$$

where  $C_0$  ( $\text{mg L}^{-1}$ ) and  $C_t$  ( $\text{mg L}^{-1}$ ) are the concentration of Pb(II) before and after adsorption;  $m$  (mg) is the mass of the PAA sponge;  $V$  (mL) is the volume of the Pb(II) solution;  $q_e$  is the adsorption capacity.

The determination of the removal efficiency and maximum adsorption capacity of Pb(II) at different dosages of the PAA sponge. PAA sponge in different dosages (2–8 mg) was added in 25 mL of 100 ppm Pb(II) solution at pH 5 and stirred at 250 rpm for 24 h. Then, 2 mL of the mixture was taken out via syringe and filtered with a  $0.45\ \mu\text{m}$  filter. The filtrate was collected for further analysis.

Adsorption kinetic studies. Briefly, 30 mL of 100 ppm Pb(II) solution was added to the 50 mL beaker, and 7.2 mg of PAA sponge was added into the solution. The mixture was stirred at 250 rpm for different times (2, 5, 10, 20, 30, 60, 120 min). Additionally, 2 mL of the mixture was taken out via syringe and filtered with a  $0.45\ \mu\text{m}$  filter. The filtrate was collected for ICP-OES measurement.

Adsorption isotherms. The adsorption isotherms were obtained by measuring the adsorption capacity of the PAA sponge at different Pb(II) concentrations (40, 60, 80, 100,

150, 200, 250 mg mL<sup>-1</sup>) at 25 °C. The pH value and volume of the solution were adjusted to 5 and 25 mL, respectively. Then, 7.5 mg of PAA sponge was added into the solution and stirred for 24 h. The mixture was taken out via syringe and filtered with a 0.45 µm filter. The filtrate was collected for further analysis.

### 3.3. Characterizations

Fourier transform infrared spectroscopy (FTIR) analyses were carried out with a Germany TENSOR type II instrument, and proton nuclear magnetic resonance (<sup>1</sup>H NMR) spectra were recorded using a Bruker AVANCE III 400 MHz spectrometer with DMSO-*d*<sub>6</sub> as a solvent. Nitrogen adsorption/desorption experiments were operated with Autosorb iQ to determine the specific surface area and pore distribution of the PAA sponge. The specific surface area of the PAA sponge was calculated with the Brunauer–Emmett–Teller (BET) method in the relative pressure ( $P/P_0$ ) range of 0.05 to 0.35, and the pore size distribution was calculated using the Barrett–Joyner–Halanda (BJH) model. Scanning electron microscope (SEM) images of the samples were observed by Hitachi Regulus 8100 at 5 kV and 10 µA. Transmission electron microscope (TEM) images were obtained by using Hitachi HT7700 with an acceleration voltage of 100 kV. X-ray photoelectron spectroscopy (XPS) spectra were received by Thermo SCIENTIFIC K-Alpha under vacuum. The concentrations of Pb(II) were determined by ICP-OES (PQ9000) and the instrument was calibrated using five standard solutions with concentrations of 0.25, 0.5, 1, 5 and 10 mg L<sup>-1</sup>.

## 4. Conclusions

In conclusion, a polymer self-assembly strategy was proposed to prepare a highly porous PAA sponge that showed abundant active functional groups for the efficient adsorption of Pb(II). The maximum adsorption capacity was 609.7 mg L<sup>-1</sup>, and the removal efficiency reached 97.2% with an adsorption capacity of 303.6 mg g<sup>-1</sup>. The adsorption kinetics study demonstrated the ultrafast adsorption of Pb(II) to reach a removal efficiency of 89.0% with an adsorption capacity of 370.7 mg g<sup>-1</sup> within 2 min, and the adsorption process can be well fitted by both pseudo-first-order and pseudo-second-order kinetic models. In addition, the adsorption isotherm study revealed that the adsorption of Pb(II) follows the Langmuir isotherm model, indicating a monolayer adsorption manner. The PAA sponge also showed excellent recyclability, with a removal efficiency up to 93% after five cycles. Furthermore, FTIR and XPS analysis revealed that the adsorption mechanism is a combination of electrostatic interaction and the coordination and complexation between Pb(II) and nitrogen and oxygen atoms. In view of the high adsorption capacity and recovery of the PAA sponge, we believe that the PAA sponge developed in this study may be a promising candidate for the efficient removal of heavy metal ions.

**Supplementary Materials:** The following supporting information can be downloaded at: <https://www.mdpi.com/article/10.3390/molecules28072897/s1>, Scheme S1. Synthesis of PAA by condensation polymerization. Figure S1. FTIR spectrum of PAA. Figure S2. <sup>1</sup>H NMR spectrum of PAA in DMSO-*d*<sub>6</sub>. Figure S3. TEM image of thin membranes formed by the self-assembly of PAA. Figure S4. Zeta potential of PAA sponge. Figure S5. (A) Nitrogen adsorption/desorption isotherm and (B) pore size distribution of PAA sponge. Figure S6. Effect of pH values on the zeta potentials of PAA sponge. Figure S7. (A) Top view and (B) side view of PAA sponge after adsorption of Pb(II). Figure S8. Effect of time on Pb(II) adsorption by PAA sponge. Figure S9. Effects of initial concentration on Pb(II) adsorption. Figure S10. XPS survey of PAA sponge. Figure S11. High-resolution Pb4f spectra of PAA sponge after adsorption of Pb(II). Figure S12. High-resolution C1s spectra of PAA sponge before and after adsorption of Pb(II).

**Author Contributions:** Conceptualization, H.S.; methodology, Y.L.; validation, Y.L. and K.J.; investigation, Y.L. and K.J.; data curation, Y.L.; writing—original draft preparation, Y.L.; writing—review and editing, T.W., X.L. and H.S.; supervision, H.S.; project administration, H.S.; funding acquisition, H.S. All authors have read and agreed to the published version of the manuscript.

**Funding:** This research was funded by the Natural Science Foundation of China, grant number U22A20119.

**Institutional Review Board Statement:** Not applicable.

**Informed Consent Statement:** Not applicable.

**Data Availability Statement:** The data that support the findings of this study are available from the corresponding author upon reasonable request.

**Acknowledgments:** H.S. thanks the Ningxia Youth Talent Support Project of Science and Technology and Young Scholars of Western China of CAS.

**Conflicts of Interest:** The authors declare no conflict of interest.

**Sample Availability:** Samples of the compounds are available from the authors.

## References

1. Gao, Y.; Deng, S.-Q.; Jin, X.; Cai, S.-L.; Zheng, S.-R.; Zhang, W.-G. The construction of amorphous metal-organic cage-based solid for rapid dye adsorption and time-dependent dye separation from water. *Chem. Eng. J.* **2019**, *357*, 129–139. [[CrossRef](#)]
2. Zhang, X.; Li, D.; Li, M.; Qin, P.; Zhu, S.; Gao, Y.; Mu, M.; Zhang, N.; Wang, Y.; Lu, M. Flower-like  $\text{Co}_3\text{O}_4/\text{C}_3\text{N}_5$  composite as solid-phase microextraction coating for high-efficiency adsorption and preconcentration of polycyclic aromatic hydrocarbons and polychlorinated biphenyls in water. *Chem. Eng. J.* **2022**, *443*, 136293. [[CrossRef](#)]
3. Cai, L.; Ying, D.; Liang, X.; Zhu, M.; Lin, X.; Xu, Q.; Cai, Z.; Xu, X.; Zhang, L. A novel cationic polyelectrolyte microsphere for ultrafast and ultra-efficient removal of heavy metal ions and dyes. *Chem. Eng. J.* **2021**, *410*, 128404. [[CrossRef](#)]
4. Bao, S.; Yang, W.; Wang, Y.; Yu, Y.; Sun, Y. One-pot synthesis of magnetic graphene oxide composites as an efficient and recoverable adsorbent for Cd(II) and Pb(II) removal from aqueous solution. *J. Hazard. Mater.* **2020**, *381*, 120914. [[CrossRef](#)]
5. Fu, F.; Wang, Q. Removal of heavy metal ions from wastewaters: A review. *J. Environ. Manag.* **2011**, *92*, 407–418. [[CrossRef](#)]
6. Atieh, M.A.; Bakather, O.Y.; Tawabini, B.; Al-Tawabini, B.; Bukhari, A.A.; Abuilaiwi, F.A.; Fettouhi, M.B. Effect of carboxylic functional group functionalized on carbon nanotubes surface on the removal of lead from water. *Bioinorg. Chem. Appl.* **2010**, *2010*, 603978. [[CrossRef](#)]
7. Singh, K.; Agarwal, M. Renu Heavy metal removal from wastewater using various adsorbents: A review. *J. Water Reuse Desalin.* **2017**, *7*, 387–419.
8. Wan, S.; Wu, J.; Zhou, S.; Wang, R.; Gao, B.; He, F. Enhanced lead and cadmium removal using biochar-supported hydrated manganese oxide (HMO) nanoparticles: Behavior and mechanism. *Sci. Total Environ.* **2018**, *616–617*, 1298–1306. [[CrossRef](#)]
9. Uddin, M.K. A review on the adsorption of heavy metals by clay minerals, with special focus on the past decade. *Chem. Eng. J.* **2017**, *308*, 438–462. [[CrossRef](#)]
10. Wang, J.; Chen, B. Adsorption and coadsorption of organic pollutants and a heavy metal by graphene oxide and reduced graphene materials. *Chem. Eng. J.* **2015**, *281*, 379–388. [[CrossRef](#)]
11. Inyang, M.; Gao, B.; Yao, Y.; Xue, Y.; Zimmerman, A.R.; Pullammanappallil, P.; Cao, X. Removal of heavy metals from aqueous solution by biochars derived from anaerobically digested biomass. *Bioresour. Technol.* **2012**, *110*, 50–56. [[CrossRef](#)]
12. Demirbas, A. Heavy metal adsorption onto agro-based waste materials: A review. *J. Hazard. Mater.* **2008**, *157*, 220–229. [[CrossRef](#)] [[PubMed](#)]
13. Ahluwalia, S.S.; Goyal, D. Microbial and plant derived biomass for removal of heavy metals from wastewater. *Bioresour. Technol.* **2007**, *98*, 2243–2257. [[CrossRef](#)] [[PubMed](#)]
14. Pan, B.; Pan, B.; Chen, X.; Zhang, W.; Zhang, X.; Zhang, Q.; Zhang, Q.; Chen, J. Preparation and preliminary assessment of polymer-supported zirconium phosphate for selective lead removal from contaminated water. *Water Res.* **2006**, *40*, 2938–2946. [[CrossRef](#)]
15. Tan, Y.; Chen, M.; Hao, Y. High efficient removal of Pb (II) by amino-functionalized  $\text{Fe}_3\text{O}_4$  magnetic nano-particles. *Chem. Eng. J.* **2012**, *191*, 104–111. [[CrossRef](#)]
16. Ren, H.; Gao, Z.; Wu, D.; Jiang, J.; Sun, Y.; Luo, C. Efficient Pb(II) removal using sodium alginate-carboxymethyl cellulose gel beads: Preparation, characterization, and adsorption mechanism. *Carbohydr. Polym.* **2016**, *137*, 402–409. [[CrossRef](#)]
17. Mei, D.; Liu, L.; Yan, B. Adsorption of uranium (VI) by metal-organic frameworks and covalent-organic frameworks from water. *Coord. Chem. Rev.* **2023**, *475*, 214917. [[CrossRef](#)]
18. Liu, Z.; Xiong, B.; Dong, Y.; Ning, Y.; Li, D. Metal–Organic Frameworks@Calcite Composite Crystals. *Inorg. Chem.* **2022**, *61*, 16203–16210. [[CrossRef](#)]
19. Yin, N.; Wang, K.; Xia, Y.A.; Li, Z. Novel melamine modified metal-organic frameworks for remarkably high removal of heavy metal Pb (II). *Desalination* **2018**, *430*, 120–127. [[CrossRef](#)]
20. Kobielska, P.A.; Howarth, A.J.; Farha, O.K.; Nayak, S. Metal–organic frameworks for heavy metal removal from water. *Coord. Chem. Rev.* **2018**, *358*, 92–107. [[CrossRef](#)]
21. Ullah, I.; Shah, A.; Khan, M.; Khan, S.Z.; ur-Rehman, Z.; Badshah, A. Synthesis and Spectrophotometric Study of Toxic Metals Extraction by Novel Thio-Based Non-Ionic Surfactant. *Tenside, Surfactants, Deterg.* **2015**, *52*, 406–413. [[CrossRef](#)]

22. Rauf, A.; Shah, A.; Abbas, S.; Rana, U.A.; Khan, S.U.; Ali, S.; Zia Ur, R.; Qureshi, R.; Kraatz, H.B.; Belanger-Gariepy, F. Synthesis, spectroscopic characterization and pH dependent photometric and electrochemical fate of Schiff bases. *Spectrochim. Acta, Part A* **2015**, *138*, 58–66. [[CrossRef](#)] [[PubMed](#)]
23. Zhu, Y.; Fan, L.; Yang, B.; Du, J. Multifunctional Homopolymer Vesicles for Facile Immobilization of Gold Nanoparticles and Effective Water Remediation. *ACS Nano* **2014**, *8*, 5022–5031. [[CrossRef](#)]
24. Zhang, S.; Zhang, Y.; Bi, G.; Liu, J.; Wang, Z.; Xu, Q.; Xu, H.; Li, X. Mussel-inspired polydopamine biopolymer decorated with magnetic nanoparticles for multiple pollutants removal. *J. Hazard. Mater.* **2014**, *270*, 27–34. [[CrossRef](#)]
25. Dupont, D.; Brullot, W.; Bloemen, M.; Verbiest, T.; Binnemans, K. Selective uptake of rare earths from aqueous solutions by EDTA-functionalized magnetic and nonmagnetic nanoparticles. *ACS Appl. Mater. Interfaces* **2014**, *6*, 4980–4988. [[CrossRef](#)]
26. Liu, Y.; Su, G.; Zhang, B.; Jiang, G.; Yan, B. Nanoparticle-based strategies for detection and remediation of environmental pollutants. *Analyst* **2011**, *136*, 872–877. [[CrossRef](#)] [[PubMed](#)]
27. Jabeen, H.; Chandra, V.; Jung, S.; Lee, J.W.; Kim, K.S.; Kim, S.B. Enhanced Cr(vi) removal using iron nanoparticle decorated graphene. *Nanoscale* **2011**, *3*, 3583–3585. [[CrossRef](#)] [[PubMed](#)]
28. Alotaibi, K.M.; Shiels, L.; Lacaze, L.; Peshkur, T.A.; Anderson, P.; Machala, L.; Critchley, K.; Patwardhan, S.V.; Gibson, L.T. Iron supported on bioinspired green silica for water remediation. *Chem. Sci.* **2017**, *8*, 567–576. [[CrossRef](#)]
29. Manos, M.J.; Kanatzidis, M.G. Metal sulfide ion exchangers: Superior sorbents for the capture of toxic and nuclear waste-related metal ions. *Chem. Sci.* **2016**, *7*, 4804–4824. [[CrossRef](#)]
30. Sun, H.; Chen, S.; Li, X.; Leng, Y.; Zhou, X.; Du, J. Lateral growth of cylinders. *Nat. Commun.* **2022**, *13*, 2170. [[CrossRef](#)]
31. Sun, H.; Zhou, X.; Leng, Y.; Li, X.; Du, J. Transformation of Amorphous Nanobowls to Crystalline Ellipsoids Induced by Trans-Cis Isomerization of Azobenzene. *Macromol. Rapid Commun.* **2022**, *43*, 2200131. [[CrossRef](#)]
32. Sun, H.; Leng, Y.; Zhou, X.; Li, X.; Wang, T. Regulation of the nanostructures self-assembled from an amphiphilic azobenzene homopolymer: Influence of initial concentration and solvent solubility parameter. *Soft Matter* **2023**, *19*, 743–748. [[CrossRef](#)] [[PubMed](#)]
33. Sun, H.; Jiang, J.; Xiao, Y.; Du, J. Efficient Removal of Polycyclic Aromatic Hydrocarbons, Dyes, and Heavy Metal Ions by a Homopolymer Vesicle. *ACS Appl. Mater. Interfaces* **2018**, *10*, 713–722. [[CrossRef](#)] [[PubMed](#)]
34. Leng, Y.; Jin, K.; Wang, T.; Sun, H. Facile Preparation of Cobalt Nanoparticles Encapsulated Nitrogen-Doped Carbon Sponge for Efficient Oxygen Reduction Reaction. *Polymers* **2023**, *15*, 521. [[CrossRef](#)]
35. Sun, H.; Jin, K.; Li, X.; Wang, T.; Lai, X. Nitrogen-doped carbon sponge derived from the self-assembly of poly(amic acid) for high performance oxygen reduction reaction. *J. Chem.* **2023**, *47*, 3297–3305. [[CrossRef](#)]
36. Yang, W.; Cao, M. Synthesis of ZIF-8@GO-COOH and its adsorption for Cu(II) and Pb(II) from water: Capability and mechanism. *Sep. Purif. Technol.* **2023**, *309*, 122957. [[CrossRef](#)]
37. Xu, X.; Ouyang, X.-k.; Yang, L.-Y. Adsorption of Pb(II) from aqueous solutions using crosslinked carboxylated chitosan/carboxylated nanocellulose hydrogel beads. *J. Mol. Liq.* **2021**, *322*, 114523. [[CrossRef](#)]
38. Wang, C.; Xiong, C.; He, Y.; Yang, C.; Li, X.; Zheng, J.; Wang, S. Facile preparation of magnetic Zr-MOF for adsorption of Pb(II) and Cr(VI) from water: Adsorption characteristics and mechanisms. *Chem. Eng. J.* **2021**, *415*, 128923. [[CrossRef](#)]
39. Liu, X.; Guan, J.; Lai, G.; Xu, Q.; Bai, X.; Wang, Z.; Cui, S. Stimuli-responsive adsorption behavior toward heavy metal ions based on comb polymer functionalized magnetic nanoparticles. *J. Clean. Prod.* **2020**, *253*, 119915. [[CrossRef](#)]
40. Wang, J.; Guo, X. Adsorption kinetic models: Physical meanings, applications, and solving methods. *J. Hazard. Mater.* **2020**, *390*, 122156. [[CrossRef](#)]
41. Ifthikar, J.; Wang, J.; Wang, Q.; Wang, T.; Wang, H.; Khan, A.; Jawad, A.; Sun, T.; Jiao, X.; Chen, Z. Highly Efficient Lead Distribution by Magnetic Sewage Sludge Biochar: Sorption Mechanisms and Bench Applications. *Bioresour. Technol.* **2017**, *238*, 399–406. [[CrossRef](#)] [[PubMed](#)]
42. Choy, K.K.H.; Porter, J.F.; McKay, G. Langmuir isotherm models applied to the multicomponent sorption of acid dyes from effluent onto activated carbon. *J. Chem. Eng. Data* **2000**, *45*, 575–584. [[CrossRef](#)]
43. Zhao, L.-X.; Song, S.-E.; Du, N.; Hou, W.-G. A sorbent concentration-dependent Freundlich isotherm. *Colloid Polym. Sci.* **2013**, *291*, 541–550. [[CrossRef](#)]
44. Langmuir, I. The adsorption of gases on plane surfaces of glass, mica and platinum. *J. Am. Chem. Soc.* **1918**, *40*, 1361–1403. [[CrossRef](#)]
45. Wang, H.; Wang, S.; Wang, S.; Tang, J.; Chen, Y.; Zhang, L. Adenosine-functionalized UiO-66-NH<sub>2</sub> to efficiently remove Pb(II) and Cr(VI) from aqueous solution: Thermodynamics, kinetics and isothermal adsorption. *J. Hazard. Mater.* **2022**, *425*, 127771. [[CrossRef](#)]
46. Taşar, Ş.; Kaya, F.; Özer, A. Biosorption of lead(II) ions from aqueous solution by peanut shells: Equilibrium, thermodynamic and kinetic studies. *J. Environ. Chem. Eng.* **2014**, *2*, 1018–1026. [[CrossRef](#)]
47. Yousif, E.; Ahmed, D.S.; Ahmed, A.; Abdallah, M.; Yusop, R.M.; Mohammed, S.A. Impact of stabilizer on the environmental behavior of PVC films reinforced 1,2,4-triazole moiety. *Environ. Sci. Pollut. Res.* **2019**, *26*, 26381–26388. [[CrossRef](#)] [[PubMed](#)]
48. Pagacz-Kostrzewa, M.; Bronisz, R.; Wierzejewska, M. Theoretical and matrix isolation FTIR studies of 3-amino-1,2,4-triazole and its isomers. *Chem. Phys. Lett.* **2009**, *473*, 238–246. [[CrossRef](#)]

49. Chen, B.; Chen, S.; Zhao, H.; Liu, Y.; Long, F.; Pan, X. A versatile  $\beta$ -cyclodextrin and polyethyleneimine bi-functionalized magnetic nanoadsorbent for simultaneous capture of methyl orange and Pb(II) from complex wastewater. *Chemosphere* **2019**, *216*, 605–616. [[CrossRef](#)]
50. He, J.; Li, Y.; Wang, C.; Zhang, K.; Lin, D.; Kong, L.; Liu, J. Rapid adsorption of Pb, Cu and Cd from aqueous solutions by  $\beta$ -cyclodextrin polymers. *Appl. Surf. Sci.* **2017**, *426*, 29–39. [[CrossRef](#)]
51. Li, X.-G.; Ma, X.-L.; Sun, J.; Huang, M.-R. Powerful Reactive Sorption of Silver(I) and Mercury(II) onto Poly(o-phenylenediamine) Microparticles. *Langmuir* **2009**, *25*, 1675–1684. [[CrossRef](#)] [[PubMed](#)]
52. Zeng, H.; Wang, L.; Zhang, D.; Yan, P.; Nie, J.; Sharma, V.K.; Wang, C. Highly efficient and selective removal of mercury ions using hyperbranched polyethylenimine functionalized carboxymethyl chitosan composite adsorbent. *Chem. Eng. J.* **2019**, *358*, 253–263. [[CrossRef](#)]
53. Xiao, D.; Ding, W.; Zhang, J.; Ge, Y.; Wu, Z.; Li, Z. Fabrication of a versatile lignin-based nano-trap for heavy metal ion capture and bacterial inhibition. *Chem. Eng. J.* **2019**, *358*, 310–320. [[CrossRef](#)]
54. Swiatkowski, A.; Pakula, M.; Biniak, S.; Walczyk, M. Influence of the surface chemistry of modified activated carbon on its electrochemical behaviour in the presence of lead(II) ions. *Carbon* **2004**, *42*, 3057–3069. [[CrossRef](#)]
55. Huang, Z.; Xiong, C.; Ying, L.; Wang, W.; Wang, S.; Ding, J.; Lu, J. Facile synthesis of a MOF-derived magnetic CoAl-LDH@chitosan composite for Pb (II) and Cr (VI) adsorption. *Chem. Eng. J.* **2022**, *449*, 137722. [[CrossRef](#)]

**Disclaimer/Publisher’s Note:** The statements, opinions and data contained in all publications are solely those of the individual author(s) and contributor(s) and not of MDPI and/or the editor(s). MDPI and/or the editor(s) disclaim responsibility for any injury to people or property resulting from any ideas, methods, instructions or products referred to in the content.